Antiparticle cloud temperatures for antihydrogen experiments

A. Bianconi,[1,2] M. Charlton,[3] E. Lodi Rizzini,[1,2] V. Mascagna,[1,2] and L. Venturelli[1,2,*]

[1]*Dipartimento di Ingegneria dell'Informazione, Università di Brescia, via Branze 38, I-25123 Brescia, Italy*

[2]*Istituto Nazionale di Fisica Nucleare, Sezione di Pavia, I-27100 Pavia, Italy*

[3]*Department of Physics, College of Science, Swansea University, Singleton Park, Swansea SA2 8PP, United Kingdom*

(Received 4 April 2017; published 18 July 2017)

A simple rate-equation description of the heating and cooling of antiparticle clouds under conditions typical of those found in antihydrogen formation experiments is developed and analyzed. We include single-particle collisional, radiative, and cloud expansion effects and, from the modeling calculations, identify typical cooling phenomena and trends and relate these to the underlying physics. Some general rules of thumb of use to experimenters are derived.

DOI: 10.1103/PhysRevA.96.013418

I. INTRODUCTION AND MOTIVATION

Since the first experiments to realize the controlled production of antihydrogen ($\overline{\mathrm{H}}$) via the mixing of clouds of positrons (e^+) and antiprotons ($\overline{p}$) [1,2] the important role of the properties of these clouds, and most notably the positron density and temperature (n_e and T_e, respectively), has been accepted. Under the conditions of most of the experiments performed to date, it is thought that the three-body reaction involving an antiproton interacting with two positrons (i.e., $\overline{p}+e^++e^+\rightarrow\overline{\mathrm{H}}+e^+$) will dominate over the radiative capture reaction, $\overline{p}+e^+\rightarrow\overline{\mathrm{H}}+h\nu$. While the rates of these two reactions scale straightforwardly with positron density as n_e^2 and n_e, respectively, their dependencies on T_e are more complex. In equilibrium, the three-body reaction is expected to vary rapidly with positron temperature as $T_e^{-4.5}$ and to produce very weakly bound states which are likely to be influenced by the electric and magnetic fields used in the experiments and by further collisions with positrons (see, e.g., [3–5] for discussions of aspects of such phenomena). By contrast, the radiative process has a much weaker dependence as $T_e^{-0.63}$, and favors formation into low-lying quantum states. More information on these basic processes, and other possible routes to $\overline{\mathrm{H}}$, can be found in relevant reviews [6–8].

Controlling T_e while manipulating the charged particle clouds for $\overline{\mathrm{H}}$ formation (which typically involves cycles of cooling and compression; see, e.g., [9–15]) is a major challenge in the quest to produce the antiatom at low enough temperatures to be held in a sub-K deep magnetic minimum trap [16–19], or for the production of well-defined beams [20,21]. Indeed, the experiments performed to date on $\overline{\mathrm{H}}$, including the first observations of ground-state hyperfine [22] and 1S-2S [23] transitions, the demonstration of a method to measure the behavior of the antiatom in the Earth's gravitational field [24], and investigations of its charge neutrality [25,26], have been achieved with a sequence of demanding runs involving small numbers of trapped $\overline{\mathrm{H}}$ atoms per cycle, from the many tens of thousands created in the e^+-$\overline{p}$ mixing. Since it is (technologically) unlikely that the depth of $\overline{\mathrm{H}}$ magnetic minimum traps can be increased much further, new methods of controlling the positron cloud temperature (for instance using sympathetic cooling via laser-cooled Be^+ ions; see [27] for a recent discussion) will need to be developed.

Though T_e is crucial, it is not a simple parameter to measure absolutely and *in situ*. Some teams have employed the method developed by the UCSD electron plasma group [28] which involves ejecting the cloud to infer, by energy analysis of the formed beam, the temperature of the trapped ensemble (e.g., [11]). This technique requires shot-to-shot stability of the cloud to allow the unmeasured T_e of the cloud used in the actual experiment to be assumed. The ATHENA collaboration developed a cloud oscillation mode diagnostic technique from which they were able to deduce changes in T_e following radio-frequency (rf) excitation [29,30], but could not directly extract its baseline value.

As a result, there are few investigations of the temperature dependence of $\overline{\mathrm{H}}$ formation, and the information that exists is somewhat confusing. For instance, by studying several measures of the $\overline{\mathrm{H}}$ yield (as a proxy for the rate of formation [31]) while T_e was raised in a range up to several thousand kelvins, ATHENA found a temperature scaling of the rate according to $T_e^{(-0.7\pm0.2)}$ [32,33]. In a later study, using a modulated rf heating technique, Fujiwara and co-workers [34] were able to model the onset of $\overline{\mathrm{H}}$ annihilation following the removal of the rf to yield a formation scaling law as $T_e^{(-1.1\pm0.5)}$.

While these T_e dependencies seem to point towards a prevalence of the radiative reaction, the instantaneous rates of $\overline{\mathrm{H}}$ formation are typically, as first noted by Amoretti and co-workers [31], at least an order of magnitude too high to be due to this capture mechanism. Furthermore, all $\overline{\mathrm{H}}$ experiments [2,11,20,35–38] have observed copious field-ionization of weakly bound states indicating, as mentioned above, that the three-body reaction dominates. This dilemma has been noted in a review of ATHENA by Amsler *et al.* [39], who have also presented some ongoing analyses of the results of that experiment.

The antiproton cloud temperature, which we denote as T_i, is also important, and there are nonequilibrium (in the sense that $T_i \neq T_e$) effects expected, which will depend upon the manner in which the $\overline{p}$'s are injected into the e^+ cloud. In the early ATHENA work [1] this was done with $\overline{p}$ kinetic energies ranging up to 15–20 eV, whereupon they slowed via collision upon repeated traversals of the cloud [38]. A subsequent study of the annihilation distributions revealed that the resulting antiatoms were predominantly nonthermal, with substantial

*luca.venturelli@unibs.it

axial speeds [40]. Accordingly, new mixing techniques were developed by ALPHA [23,41] to reduce this effect to promote $\overline{\mathrm{H}}$ formation with the lowest feasible kinetic energies to ensure that some antiatoms were available for trapping.

Not all of the phenomena that can affect T_e and T_i were fully appreciated during the early $\overline{\mathrm{H}}$ experiments. While ATHENA's absolute positron temperatures in their so-called "cold mixing" experiments were unknown, typical values of n_e were in the range 10^{14}–10^{15} m^{-3}. It has been pointed out several times elsewhere (e.g., [4,5]) that the self-electric field, E_r, of the positron cloud, which is radial (r) in nature and is proportional to $n_e r$, in combination with the axial magnetic field, B_z, used to confine the charged particles, results in a tangential speed $v_t = E_r/B_z$ which, to first order, is independent of particle mass and which can impart substantial additional kinetic energy (over thermal) to the nascent $\overline{\mathrm{H}}$. Furthermore, as elucidated in most detail in [5], the formation of observable $\overline{\mathrm{H}}$ consists of a sequence of events in which a $\overline{p}$ transiently captures a e^+ which is then rapidly ionized by a further collision. A major result of this is a net radial diffusion of the $\overline{p}$'s, which occurs while they are paired with positrons, towards the outer edge of the cloud. Since the probability of transient $\overline{\mathrm{H}}$ formation is driven by the three-body reaction, the diffusion rate is strongly n_e and T_e dependent [5]. The upshot is that the $\overline{\mathrm{H}}$ that is observed may have been formed at a significantly larger radial position in the e^+ cloud than the original $\overline{p}$ injection radius. This will presumably lead to larger kinetic energies on formation, and which may be in the 10's of K region.

Effects such as this have motivated the use of lower positron densities (see, e.g., [16–18]), but still with the need to maintain $\overline{p}$ numbers to provide a reasonable antihydrogen yield, whether in a trap or a beam. Thus, it is not just T_e and T_i that can affect the final $\overline{\mathrm{H}}$ speed, but also, indirectly, n_e. Furthermore, the aforementioned $\overline{p}$ radial diffusion effect also means that $\overline{\mathrm{H}}$ that can be trapped, or usefully manipulated into a beam, is most likely to be formed shortly after the $\overline{p}$ and e^+ clouds have been mixed, provided that they have had sufficient time to reach thermal equilibrium. Such time scales are those that we consider foremost in the present study.

In addition to their $\overline{\mathrm{H}}$ work, ATHENA has also reported observations consistent with the formation of low-energy protonium, Pn, the proton-$\overline{p}$ bound state [42,43]. Ongoing analyses of the relevant data, which include examination of spatial $\overline{p}$ annihilation distributions, encompass dynamical effects, which provide further motivation for our study.

Within a few years, CERN's unique $\overline{p}$ facility, the Antiproton Decelerator (AD) [44,45], will be augmented with ELENA, an extralow-energy ring [46]. ELENA will take the AD output $\overline{p}$'s at 5.3 MeV kinetic energy and slow them down to about 100 keV. The resultant ejected beam can be captured with around 2 orders of magnitude increase in efficiency by the experiments which could, if desired, provide much larger $\overline{p}$ pulses for $\overline{\mathrm{H}}$ work. The implied large increase in the ratio of the numbers of $\overline{p}$'s to e^+'s, N_i/N_e, may radically influence cooling and thermalization, and this has also motivated our work.

Our goal has been to develop a simple and easily applicable model of the behavior of $\overline{p}$ and e^+ temperatures under conditions similar to those found in $\overline{\mathrm{H}}$ and related experimentation—past, present, and future. In doing so we have taken the known phenomena which influence T_e and T_i and combined them in a self-consistent analysis, which has allowed us to identify major trends and scalings and to provide useful guidance for experiment. In the following section we present a resumé of the model, including the experimental parameters and systematics that we have used as input to the calculations. Section III gives the main results and a discussion of some of the implications, with concluding remarks to be found in Sec. IV.

II. RESUMÉ AND SCOPE OF THE MODEL

In this section we summarize our approach. The basic model we use was described in a previous report [47], and we will refer as appropriate to that work. We note, though, that the analysis and results presented in Sec. III constitute the main importance of this work, when compared to [47]. We start from a presumed e^+ cloud base temperature [$T_e(0)$], which can be varied, but which here we take as the environment, or reservoir temperature, T_{res}, and include the following phenomena: (i) When $\overline{p}$'s are injected into the positrons their kinetic energy, which is dissipated by collisions, causes the cloud to heat. (ii) If the e^+ cloud is expanding with time, then the conversion of electrostatic self-energy also results in heating of the ensemble. (iii) These effects are mitigated by the cooling effect provided by the emission of synchrotron radiation by the e^+ in the strong solenoidal fields present. All three effects have been combined [47] into a set of rate equations for T_i and T_e (which can also include effects due to imperfect cloud overlap [47], though these are ignored here) whose solution yields the time dependence of the temperatures of both species, but in particular T_e. While the heating and cooling effects are all understood, to the best of our knowledge they have only been combined into a single self-consistent model in [47] and in the present work.

At the outset we note, following the analysis in [47], that we only consider the so-called nonmagnetized situation in which a single global temperature T_e can be assigned to the positrons. In other words, we have steered clear of the conditions that result in the loss of transverse freedom when electrons and positrons are confined at low cloud temperatures in high magnetic fields: these arise at temperatures below approximately 10 K for magnetic fields of 3 T and higher (see Fig. 1 of [47]). On the other hand the presence of the magnetic field is taken into account in the present work using, as described below, a description of ion cooling. The range of n_e considered spans those employed in $\overline{\mathrm{H}}$ experiments, both past and ongoing.

The quantities we consider in the model are as follows: the kinetic energy of injection of the $\overline{p}$'s into the e^+ cloud [$E_i(0)$, or its temperature equivalent, $T_i(0)$]; the initial radius and density of this cloud and its radial expansion speed, dr_e/dt; the ratio $\epsilon = N_i/N_e$ of the numbers of antiprotons (N_i) and positrons (N_e) used to form $\overline{\mathrm{H}}$; as mentioned above, an assumed $T_e(0) = T_{\mathrm{res}}$ and the aforementioned reservoir temperature T_{res}, which is typically that of the surrounding charged particle traps. We are able to vary the input parameters at will, and have explored ranges of positron density and radial expansion speed to gauge their effect on T_e.

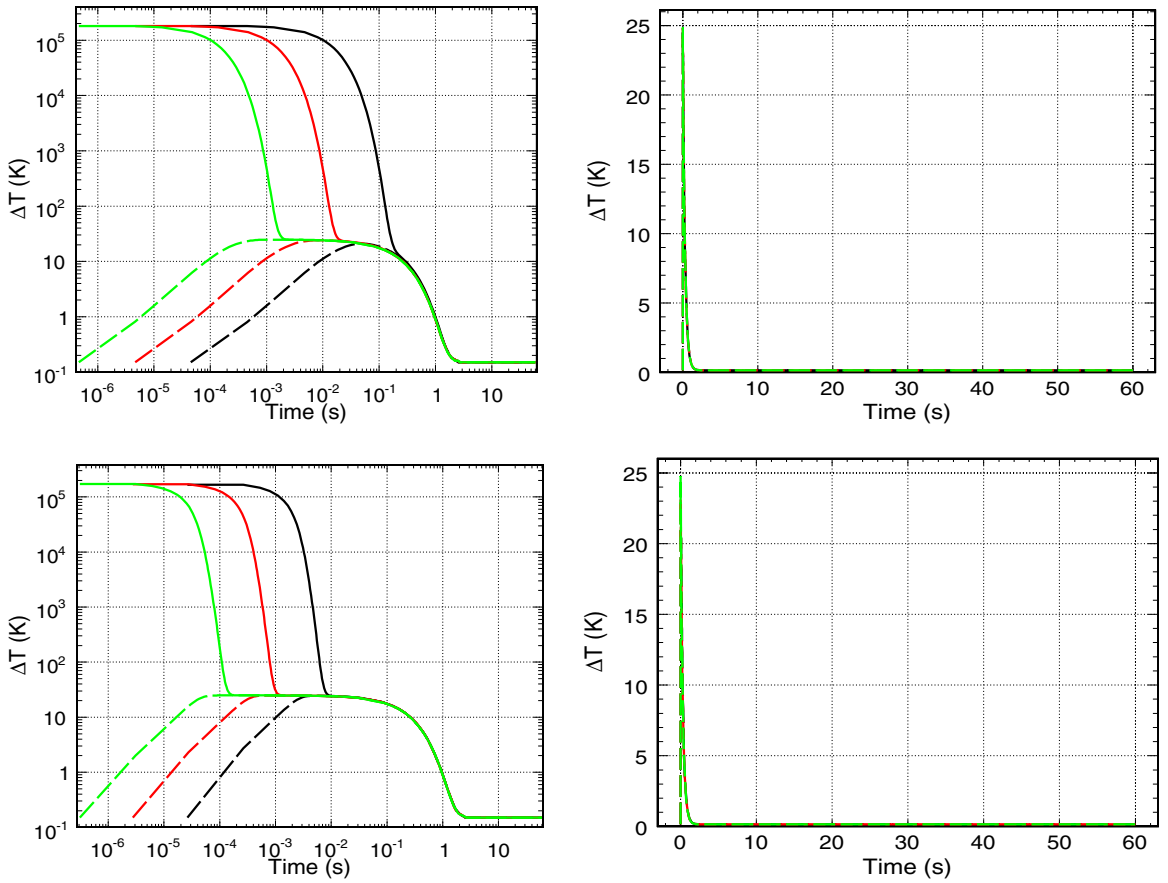

FIG. 1. Comparison of the time dependencies of the change in temperature ΔT [which are $\Delta T_e(t)$ and $\Delta T_i(t)$ as appropriate; see text] of the positron (dashed lines) and antiproton (full lines) clouds for the Spitzer (upper panes) and Hurt *et al.* (lower panes) ion cooling terms. The densities, n_e, investigated are 7×10^{13} (black), 7×10^{14} (red), and 7×10^{15} m^{-3} (green), here all shown for $dr_e/dt = 0$, and with $\epsilon = 10^{-4}$ and $E_i(0) = 15$ eV.

To compute the time dependence of the temperature of the antiprotons and positrons on mixing, we solve the following pair of equations,

$$\frac{dT_i}{dt} = -\frac{1}{\tau_i}(T_i - T_e) \tag{1}$$

and

$$\frac{dT_e}{dt} = \frac{1}{\tau_i}\epsilon(T_i - T_e) - \frac{(T_e - T_{\rm res})}{\tau_e} + \frac{e^2}{6\varepsilon_0 k_B}\left(n_e {r_e}^2\right)_0 \frac{1}{r_e}\frac{dr_e}{dt}. \tag{2}$$

τ_i is usually taken to be the standard Spitzer collisional damping time for an ion ($\overline{p}$) interacting with a positron (or

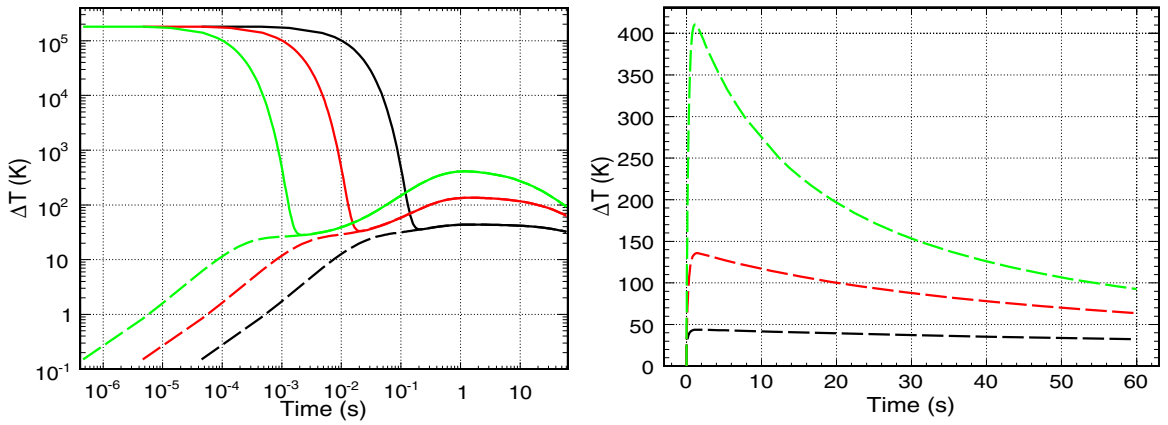

FIG. 2. The time dependencies of ΔT [which are $\Delta T_e(t)$ and $\Delta T_i(t)$ as appropriate; see text] for antiprotons and positrons using the term of Hurt *et al.* for τ_i. The curve coding and parameters are as for Fig. 1, except that here $u \neq 0$ since $dr_e/dt = 2 \times 10^{-5}$ m s^{-1}.

electron) cloud [47,48]. As described in Sec. III, we have compared the behaviors of T_e and T_i using the Spitzer result for τ_i with those found using the simple empirical function of Hurt and co-workers [49], namely that $\tau_i = 1/2n_e\gamma$, with $\gamma = 4.3 \times 10^{-12}/B_z$ m^3 s^{-1}, with B_z in units of teslas. As a result of this comparison we have used Hurt's function for the data presented herein. That expression was derived as a result of an analysis of antiproton-positron collisions in the presence of a strong magnetic field and, as such, is more applicable to the antihydrogen formation scenario described herein.

Equation (1) describes the behavior of T_i as the $\overline{p}$'s cool towards T_e following injection into the e^+ cloud. Equation (2) describes the temporal behavior of T_e and contains terms due to the heating caused by the injection of N_i $\overline{p}$'s into the positrons, the cooling of the latter due to the emission of synchrotron radiation with a time constant $\tau_e = 3\pi\varepsilon_0 m_e^3 c^3/e^4 B_z^2$ (with c the speed of light, ε_0 the permittivity of free space, and e and m_e the charge and mass, respectively, of the e^+), and the electrostatic heating of the positron cloud by radial expansion [50]. Since the length of the plasma remains constant the quantity $(n_e r_e^2)_0$ is also approximately constant at its value at the start of the mixing experiment. We ignore the depletion in N_e (and the concomitant reduction in density) due to antihydrogen formation, which in the worst case studied here is under 10%, and is typically much less. The experimental information needed to make this correction is not readily available, and any model-based attempt to do so would be heavily dependent upon assumptions that would not be easy to justify. Similarly, we do not take into account loss of N_i as a result of antihydrogen creation, or radial transport [4,5]. Though the fractional loss of the $\overline{p}$'s may be considerably higher than for the positrons (since typically $\epsilon \ll 1$), the reduction in N_i will predominantly occur once the $\overline{p}$ and e^+ are at, or close to, thermal equilibrium and as such will not materially affect the main conclusions of our work. Writing, for compactness, $u = \frac{e^2}{6\varepsilon_0 k_B}(n_e r_e^2)_0 \frac{1}{r_e}\frac{dr_e}{dt}$ in what follows we consider Eq. (2) in the form

$$\frac{dT_e}{dt} = \epsilon\frac{(T_i - T_e)}{\tau_i} - \frac{(T_e - T_{\rm res})}{\tau_e} + u. \qquad (3)$$

III. RESULTS AND DISCUSSION

In this section we present the results of our analysis for various input parameters, and describe the main physical features we find in terms of the time scales involved, and the temporal behavior of the various terms in Eq. (3). We stress, though, that this is foremost a numerical analysis, and that the data we present constitutes our main output. The parameter range we have considered are values of n_e between 1×10^{12} and 1×10^{16} m^{-3}, B_z of 2 and 3 T, $E_i(0)$ from 1.5–30 eV, and ϵ in the range 10^{-1} to 10^{-4}. The initial value of the radius r_e of the positron plasma has been fixed at 1 mm.

Figure 1 shows the modeled behavior of $T_e(t)$ and $T_i(t)$ [in fact we consider the quantity $\Delta T_e(t) = T_e(t) - T_{\rm res}$, which has the same behavior as $T_e(t)$, and its antiproton equivalent, $\Delta T_i(t)$] for three values of n_e in the range from 7×10^{13} to 7×10^{15} m^{-3} and with $dr_e/dt = 0$ for both the Spitzer and Hurt *et al.* expressions for τ_i. Aside from differences in time scale, the main features of the $\overline{p}$ cooling and e^+ heating curves are similar in both cases. We have found this to be consistently so (even when $dr_e/dt \neq 0$), and adopting the formula of Hurt *et al.* for τ_i allows us to draw some simple conclusions regarding the form of these curves. Furthermore that formulation, which was developed with antihydrogen experiments in mind, includes, as noted above, the magnetic field B_z, and as such is more appropriate here. Inserting numbers for τ_e and τ_i we find $\tau_i \approx 1.2 \times 10^{-3} B_z/n_e$ (s), with n_e in units of 10^{14} m^{-3} and $\tau_e \approx 2.6/B_z^2$ (s). These time scales are equal when $B_z^3/n_e \approx 2.2 \times 10^{-11}$ T^3 m^3, which for magnetic fields typical of $\overline{\rm H}$ experiments to date occurs at n_e of 10^{12} m^{-3} or lower. Thus, we can assume, for most situations of practical relevance, that $\tau_i \ll \tau_e$.

Figure 2 is an example of the cooling and heating curves for $u \neq 0$ (and in particular here for $dr_e/dt = 2 \times 10^{-5}$ m s^{-1})

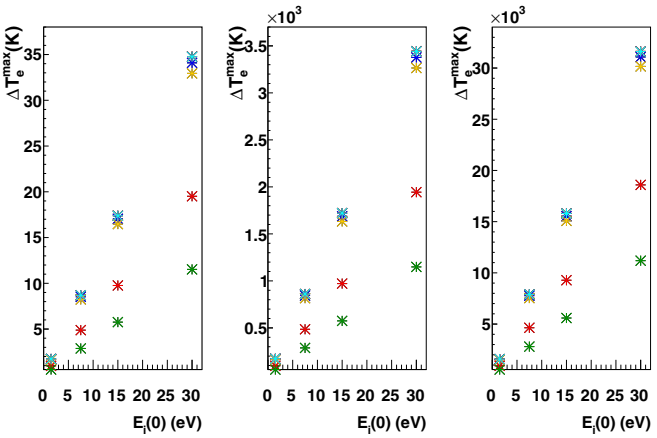

FIG. 3. Variation of the maximum positron temperature, $\Delta T_e^{\rm max}$, versus antiproton injection kinetic energy for various values of ϵ, and for $u = 0$: left panel, $\epsilon = 10^{-4}$, central panel, $\epsilon = 10^{-2}$, and right panel, $\epsilon = 10^{-1}$. Key: red, $B_z = 2$ T and $n_e = 10^{12}$ m^{-3}; green, $B_z = 3$ T and $n_e = 10^{12}$ m^{-3}; blue, $B_z = 2$ T and $n_e = 10^{14}$ m^{-3}; orange, $B_z = 3$ T and $n_e = 10^{14}$ m^{-3}; pink, $B_z = 2$ T and $n_e = 10^{16}$ m^{-3}; cyan, $B_z = 3$ T and $n_e = 10^{16}$ m^{-3}.

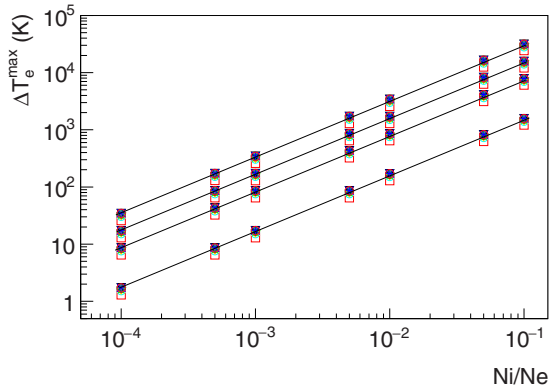

FIG. 4. Variation of the maximum positron temperature, $\Delta T_e^{\rm max}$, versus ϵ at various input kinetic energies, $E_i(0)$, and for $u = 0$. The lines shown are indicative to draw attention to data trends. The lower line is for $E_i(0) = 1.5$ eV, while the upper corresponds to 30 eV. The intermediate data sets are for 7.5 and 15 eV. For clarity, see Fig. 5 for the key.

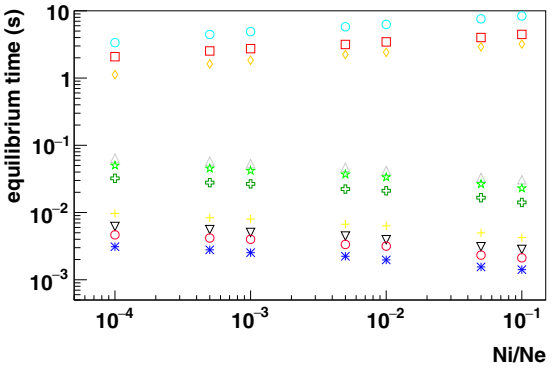

FIG. 5. The time to reach equilibrium (see text) versus ϵ for $E_i(0) = 15$ eV and $u = 0$. Key: cyan ◯ $B_z = 2$ T and $n_e = 10^{13}$ m^{-3}; □ $B_z = 3$ T and $n_e = 10^{13}$ m^{-3}; △ $B_z = 2$ T and $n_e = 5 \times 10^{13}$ m^{-3}; ◇ $B_z = 3$ T and $n_e = 5 \times 10^{13}$ m^{-3}; + $B_z = 2$ T and $n_e = 10^{14}$ m^{-3}; ⋆ $B_z = 3$ T and $n_e = 10^{14}$ m^{-3}; ▽ $B_z = 2$ T and $n_e = 5 \times 10^{14}$ m^{-3}; + $B_z = 3$ T and $n_e = 5 \times 10^{14}$ m^{-3}; ∗ $B_z = 2$ T and $n_e = 10^{15}$ m^{-3}; red ◯ $B_z = 3$ T and $n_e = 10^{15}$ m^{-3}.

showing that, if it is large enough, the heating term has a significant effect at long times: in this case the positron and antiproton temperature are still dropping even after 60 s. Inspection of both Figs. 1 and 2 shows that it is plausible (and this is borne out by numerical evaluations) to divide the analysis of the behavior of the cloud temperatures into a hierarchy of three time ranges, which we label simply using times t_A, t_B, and t_C. The range $t \leqslant t_A$ is characterized by a rapid drop in $\overline{p}$ temperature upon mixing with a cold positron cloud, accompanied by a rise in T_e as the two temperatures approach convergence. Here the first term on the right-hand side of Eq. (3) is dominant, and it is useful to proceed at short times by ignoring the other two terms. (Note that this entails setting $u = 0$, which corresponds to our simulations with $dr_e/dt = 0$.) For much of the time range $t \leqslant t_A$ we have $T_i \gg T_e$ such that Eq. (1) simplifies to $dT_i/dt = -T_i/\tau_i$, with the trivial solution $T_i(t) = T_i(0)e^{-t/\tau_i}$. Similarly, Eq. (3) can be written, $dT_e/dt = \epsilon T_i/\tau_i$, and since at $t = 0, \Delta T_e = 0$ it is straightforward to show that $\Delta T_e(t) = \epsilon T_i(0)(1 - e^{-t/\tau_i})$. Thus, for this case, $\Delta T_e \to \epsilon T_i(0) = \Delta T_e^{\max}$ for $t \gg \tau_i$. As such, the curves show a near-exponential drop in T_i, with a similar rise in T_e (scaled by ϵ).

Figure 3 shows the behavior of $\Delta T_e^{\max}$ versus the initial $\overline{p}$ kinetic energy [expressed in eV as $E_i(0) = k_B T_i(0)/e$] at various n_e and B_z for $u = 0$. For densities above about 10^{13} m^{-3} $\Delta T_e^{\max} \approx \epsilon T_i(0)$, irrespective of n_e and B_z. This is in accord with the analysis above, since the $\overline{p}$ cooling term is dominant. At the lowest density we have studied (10^{12} m^{-3}) τ_e and τ_i are comparable such that there is a noticeable effect of B_z on $\Delta T_e^{\max}$, which is also lower than at the higher densities due to the effect of the synchrotron cooling. The effect of ϵ on $\Delta T_e^{\max}$ for various n_e and $T_i(0)$, is shown in Fig. 4, with the strict proportionality to ϵ evident in all cases.

We now consider the intermediate time phase $t_A \lesssim t \lesssim t_B$, with $\Delta T_e = \Delta T_e^{\max}$ at $t = t_A$. Here the effects of the heating term are, in most cases, still not important, so again setting $u = 0$ and with $T_e - T_i \approx 0$, Eq. (3) yields the simple solution $\Delta T_e(t) = T_e^{\max} e^{-(t-t_A)/\tau_e}$. By matching up the short ($t \lesssim t_A$) and intermediate ($t_A \lesssim t \lesssim t_B$) time solutions we may guess a composite functional form for $\Delta T_e(t)$ as

$$\Delta T_e(t) \approx [\epsilon T_i(0)(1 - e^{-t/\tau_i})]e^{-(t-t_A)/\tau_e}, \tag{4}$$

such that the maximum in ΔT_e occurs at

$$t_{\max} = \tau_i \ln\left(1 + \frac{\tau_e}{\tau_i}\right) \approx \tau_i \ln\left(\frac{\tau_e}{\tau_i}\right), \tag{5}$$

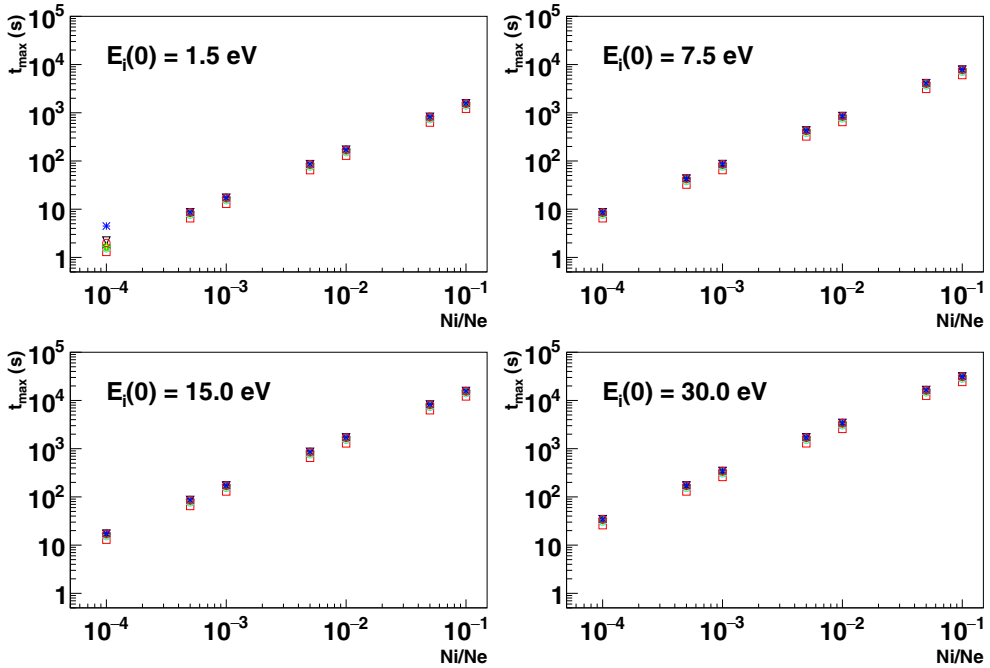

FIG. 6. The time to reach maximum positron temperature $t_{\max}$ versus ϵ for various $E_i(0)$ and with $dr_e/dt = 2 \times 10^{-7}$ m s^{-1}. Key: as for Fig. 5.

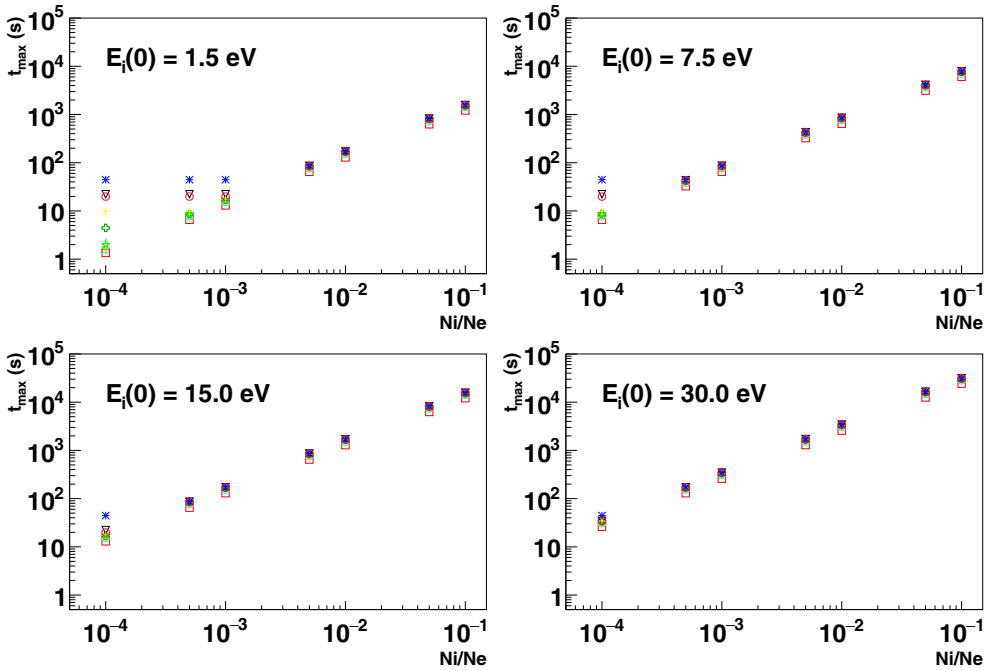

FIG. 7. The time to reach maximum positron temperature $t_{\max}$ versus ϵ for various $E_i(0)$ and with $dr_e/dt = 2 \times 10^{-6}$ m s^{-1}. Key: as for Fig. 5.

which is independent of ϵ, in accord with the modeling data. The model asserts that $t_{\max}$ is inversely proportional to n_e (in accord with the result of Hurt *et al.* for τ_i), and is approximately 2–3 $\times 10^{12}/n_e$ (s), except at the lowest densities, where it is shorter due to the effect of the cloud cooling.

Furthermore, the time to reach equilibrium (when $T_e = T_i = T_{\rm res}$ for the case with $dr_e/dt = 0$) scales with density roughly as $4 \times 10^{12}/n_e$ (s) above about 10^{13} m^{-3}, but is longer at lower densities by a factor which rises somewhat with increased ϵ (for instance it is about 4 times higher for $\epsilon = 10^{-1}$); see Fig. 5. Clearly, this is due to the increased heating of the positron cloud by the more numerous $\overline{p}$'s. The times to reach the maximum $\Delta T_e^{\max}$, and that to reach equilibrium, are independent of $E_i(0)$ in the range 1.5–30 eV.

In the third time phase ($t \gtrsim t_B$), the expansion and (re)heating term is important, so now we consider the second and third terms of Eq. (3) which can be solved to yield

$$\Delta T_e(t) = \Delta T_e^{\max} e^{-t/\tau_e} + u\tau_e(1 - e^{-t/\tau_e}) \quad t > t_B, \quad (6)$$

such that the drop in T_e due to the heat exchange with the reservoir is followed by a rise to a constant asymptotic value $\Delta T_e(t) \approx \Delta T_e(\infty) = u\tau_e$ for $t \gg \tau_e$. To further justify the division into gross time phases we evaluate the third term in Eq. (2) to find approximately $3.4 n_e dr_e/dt$ K s^{-1} with n_e in units of 10^{14} m^{-3} and dr_e/dt in 10^{-6} m s^{-1}. We have considered cloud expansion rates around this value since cloud sizes are typically in the mm range, and antiparticle handling and mixing cycles may be up to 100 s long. Our data indicate that for $\epsilon \geqslant 10^{-2}$, the behavior is identical to that for zero cloud expansion, and that this is due to the dominance of the first term in Eq. (3). However, at lower values of ϵ the third term becomes important, and this effect is seen in the behavior of $\Delta T_e^{\max}$ at $\epsilon = 10^{-4}$ as shown in Fig. 6 and, in particular, Fig. 7, and is most noticeable at low values of $E_i(0)$.

For $dr_e/dt = 2 \times 10^{-7}$ m s^{-1} and at the high e^+ cloud density of 10^{16} m^{-3} with $B_z = 2$ T, $\Delta T_e^{\max}$ is independent of $E_i(0)$, since the plasma expansion term dominates. This effect is partially curtailed at higher $E_i(0)$ when $B_z = 3$ T due to the increased synchrotron cooling rate. At the higher cloud expansion rate of 2×10^{-6} m s^{-1} there are dramatic increases in $\Delta T_e^{\max}$ of hundreds of kelvins when $\epsilon = 10^{-4}$ for $n_e = 10^{16}$ m^{-3}, which is also independent of $E_i(0)$.

IV. CONCLUSIONS

We have presented some of the salient results of our numerical modeling of the time dependencies of the temperatures of interacting antiparticle clouds whose properties are similar to those currently used in antihydrogen experiments. Our model incorporates antiproton-positron energy exchange (following injection of the former at a fixed, though variable, kinetic energy into the latter) and synchrotron cooling of the positrons in the strong magnetic fields used for charged particle confinement. Furthermore, we have the capability to incorporate positron cloud expansion whereby conversion of electrostatic self-energy leads to heating of the cloud. We have found it convenient, and physically motivated by our data, to divide the time scale of the model into three regions. The small times are dominated by antiproton energy loss, with the accompanying positron heating. At intermediate times the synchrotron cooling term becomes important, and finally, if $dr_e/dt \neq 0$, at long times the heating via cloud expansion comes into play, and can, if it is large enough, markedly influence the approach to equilibrium.

We summarize our main findings as follows:

(1) The Spitzer and Hurt *et al.* expressions for τ_i give the same qualitative features for the cooling curves.

(2) When dr_e/dt is above about 10^{-6} m s^{-1}, the cloud expansion leads to prolonged nonthermal effects that are exacerbated at high n_e.

(3) The rise in the positron temperature, ΔT_e, reaches a maximum given by the initial antiproton temperature, scaled by ϵ, the antiproton to positron ratio, and above positron densities of 10^{13} m^{-3} there is no dependence on n_e or the axial magnetic field, B_z.

(4) The time, in seconds, to reach the maximum positron temperature is given approximately by 2–3 $\times$ $10^{12}/n_e$.

We hope that these general rules will be of some value to co-workers, and that they will be of assistance in ongoing programs, both in laboratory work and in the data analysis of completed experiments.

ACKNOWLEDGMENT

We are grateful for support for this work from the EPSRC (UK) and INFN (Italy).

[1] M. Amoretti *et al.* (ATHENA Collaboration), Nature (London) **419**, 456 (2002).
[2] G. Gabrielse, N. S. Bowden, P. Oxley, A. Speck, C. H. Storry, J. N. Tan, M. Wessels, D. Grzonka, W. Oelert, G. Schepers, T. Sefzick, J. Walz, H. Pittner, T. W. Hansch, and E. A. Hessels (ATRAP Collaboration), Phys. Rev. Lett. **89**, 213401 (2002).
[3] F. Robicheaux, J. Phys. B **41**, 192001 (2008).
[4] S. Jonsell, D. P. van der Werf, M. Charlton, and F. Robicheaux, J. Phys. B **42**, 215002 (2009).
[5] S. Jonsell, M. Charlton, and D. P. van der Werf, J. Phys. B **49**, 134004 (2016).
[6] M. H. Holzscheiter, M. Charlton, and M. M. Nieto, Phys. Rep. **402**, 1 (2004).
[7] A. Müller and A. Wolf, Hyperfine Interact. **109**, 233 (1997).
[8] G. Gabrielse, Adv. At., Mol., Opt. Phys. **50**, 155 (2005).
[9] G. Gabrielse, X. Fei, L. A. Orozco, R. L. Tjoelker, J. Haas, H. Kalinowsky, T. A. Trainor, and W. Kells (TRAP Collaboration), Phys. Rev. Lett. **65**, 1317 (1990).
[10] X. Feng *et al.*, Hyperfine Interact. **109**, 145 (1997).
[11] G. B. Andresen *et al.* (ALPHA Collaboration), Phys. Lett. B **685**, 141 (2010).
[12] G. Gabrielse, W. S. Kolthammer, R. McConnell, P. Richerme, R. Kalra, E. Novitski, D. Grzonka, W. Oelert, T. Sefzick, M. Zielinski, D. Fitzakerley, M. C. George, E. A. Hessels, C. H. Storry, M. Weel, A. Mullers, and J. Walz (ATRAP Collaboration), Phys. Rev. Lett. **106**, 073002 (2011).
[13] G. Manfredi and P.-A. Hervieux, Phys. Rev. Lett. **109**, 255005 (2012).
[14] G. B. Andresen, W. Bertsche, P. D. Bowe, C. C. Bray, E. Butler, C. L. Cesar, S. Chapman, M. Charlton, J. Fajans, M. C. Fujiwara, R. Funakoshi, D. R. Gill, J. S. Hangst, W. N. Hardy, R. S. Hayano, M. E. Hayden, R. Hydomako, M. J. Jenkins, L. V. Jorgensen, L. Kurchaninov, R. Lambo, N. Madsen, P. Nolan, K. Olchanski, A. Olin, A. Povilus, P. Pusa, F. Robicheaux, E. Sarid, S. Seif El Nasr, D. M. Silveira, J. W. Storey, R. I. Thompson, D. P. van der Werf, J. S. Wurtele, and Y. Yamazaki (ALPHA Collaboration), Phys. Rev. Lett. **100**, 203401 (2008).
[15] N. Kuroda, H. A. Torii, M. Shibata, Y. Nagata, D. Barna, M. Hori, D. Horvath, A. Mohri, J. Eades, K. Komaki, and Y. Yamazaki, Phys. Rev. Lett. **100**, 203402 (2008).
[16] G. B. Andresen *et al.* (ALPHA Collaboration), Nature (London) **468**, 673 (2010).
[17] G. B. Andresen *et al.* (ALPHA Collaboration), Nat. Phys. **7**, 558 (2011).
[18] G. B. Andresen *et al.* (ALPHA Collaboration), Phys. Lett. B **695**, 95 (2011).
[19] G. Gabrielse, R. Kalra, W. S. Kolthammer, R. McConnell, P. Richerme, D. Grzonka, W. Oelert, T. Sefzick, M. Zielinski, D. W. Fitzakerley, M. C. George, E. A. Hessels, C. H. Storry, M. Weel, A. Mullers, and J. Walz (ATRAP Collaboration), Phys. Rev. Lett. **108**, 113002 (2012).
[20] Y. Enomoto, N. Kuroda, K. Michishio, C. H. Kim, H. Higaki, Y. Nagata, Y. Kanai, H. A. Torii, M. Corradini, M. Leali, E. Lodi-Rizzini, V. Mascagna, L. Venturelli, N. Zurlo, K. Fujii, M. Ohtsuka, K. Tanaka, H. Imao, Y. Nagashima, Y. Matsuda, B. Juhasz, A. Mohri, and Y. Yamazaki, Phys. Rev. Lett. **105**, 243401 (2010).
[21] N. Kuroda *et al.*, Nat. Commun. **5**, 3089 (2014).
[22] C. Amole *et al.* (ALPHA Collaboration), Nature (London) **483**, 439 (2012).
[23] M. Ahmadi *et al.* (ALPHA Collaboration), Nature (London) **541**, 506 (2017).
[24] C. Amole *et al.* (ALPHA Collaboration), Nat. Commun. **4**, 1785 (2013).
[25] C. Amole *et al.* (ALPHA Collaboration), Nat. Commun. **5**, 3955 (2014).
[26] M. Ahmadi *et al.* (ALPHA Collaboration), Nature (London) **529**, 373 (2016).
[27] N. Madsen, F. Robicheaux, and S. Jonsell, New J. Phys. **16**, 063046 (2014).
[28] D. L. Eggleston, C. F. Driscoll, B. R. Beck, A. W. Hyatt, and J. H. Malmberg, Phys. Fluids. **4**, 3432 (1992).
[29] M. Amoretti, C. Amsler, G. Bonomi, A. Bouchta, P. Bowe, C. Carraro, C. L. Cesar, M. Charlton, M. Doser, V. Filippini, A. Fontana, M. C. Fujiwara, R. Funakoshi, P. Genova, J. S. Hangst, R. S. Hayano, L. V. Jorgensen, V. Lagomarsino, R. Landua, D. Lindelof, E. L. Rizzini, M. Macri, N. Madsen, G. Manuzio, P. Montagna, H. Pruys, C. Regenfus, A. Rotondi, G. Testera, A. Variola, and D. P. van der Werf (ATHENA Collaboration), Phys. Rev. Lett. **91**, 055001 (2003).
[30] M. Amoretti *et al.* (ATHENA Collaboration), Phys. Plasmas **10**, 3056 (2003).
[31] M. Amoretti *et al.* (ATHENA Collaboration), Phys. Lett. B **578**, 23 (2004).
[32] M. Amoretti *et al.* (ATHENA Collaboration), Phys. Lett. B **583**, 59 (2004).
[33] G. Bonomi *et al.* (ATHENA Collaboration), Nucl. Instrum. Methods Phys. Res. B **214**, 17 (2004).

[34] M. C. Fujiwara, M. Amoretti, C. Amsler, G. Bonomi, A. Bouchta, P. D. Bowe, C. Canali, C. Carraro, C. L. Cesar, M. Charlton, M. Doser, A. Fontana, R. Funakoshi, P. Genova, J. S. Hangst, R. S. Hayano, L. V. Jorgensen, A. Kellerbauer, V. Lagomarsino, R. Landua, E. Lodi-Rizzini, M. Macri, N. Madsen, G. Manuzio, D. Mitchard, P. Montagna, H. Pruys, C. Regenfus, A. Rotondi, G. Testera, A. Variola, L. Venturelli, D. P. van der Werf, Y. Yamazaki, and N. Zurlo (ATHENA Collaboration), Phys. Rev. Lett. **101**, 053401 (2008).

[35] G. Gabrielse, N. S. Bowden, P. Oxley, A. Speck, C. H. Storry, J. N. Tan, M. Wessels, D. Grzonka, W. Oelert, G. Schepers, T. Sefzick, J. Walz, H. Pittner, T. W. Hasch, and E. A. Hessels (ATRAP Collaboration), Phys. Rev. Lett. **89**, 233401 (2002).

[36] D. Vrinceanu, B. E. Granger, R. Parrott, H. R. Sadeghpour, L. Cederbaum, A. Mody, J. Tan, and G. Gabrielse, Phys. Rev. Lett. **92**, 133402 (2004).

[37] T. Pohl, H. R. Sadeghpour, and G. Gabrielse, Phys. Rev. Lett. **97**, 143401 (2006).

[38] M. Amoretti *et al.* (ATHENA Collaboration), Phys. Lett. B **590**, 133 (2004).

[39] C. Amsler *et al.*, Int. J. Mod. Phys. A **29**, 1430035 (2014).

[40] N. Madsen, M. Amoretti, C. Amsler, G. Bonomi, P. D. Bowe, C. Carraro, C. L. Cesar, M. Charlton, M. Doser, A. Fontana, M. C. Fujiwara, R. Funakoshi, P. Genova, J. S. Hangst, R. S. Hayano, L. V. Jorgensen, A. Kellerbauer, V. Lagomarsino, R. Landua, E. Lodi-Rizzini, M. Macri, D. Mitchard, P. Montagna, H. Pruys, C. Regenfus, A. Rotondi, G. Testera, A. Variola, L. Venturelli, D. P. van der Werf, Y. Yamazaki, and N. Zurlo (ATHENA Collaboration), Phys. Rev. Lett. **94**, 033403 (2005).

[41] G. B. Andresen, M. D. Ashkezari, M. Baquero-Ruiz, W. Bertsche, P. D. Bowe, E. Butler, P. T. Carpenter, C. L. Cesar, S. Chapman, M. Charlton, J. Fajans, T. Friesen, M. C. Fujiwara, D. R. Gill, J. S. Hangst, W. N. Hardy, M. E. Hayden, A. J. Humphries, J. L. Hurt, R. Hydomako, S. Jonsell, N. Madsen, S. Menary, P. Nolan, K. Olchanski, A. Olin, A. Povilus, P. Pusa, F. Robicheaux, E. Sarid, D. M. Silveira, C. So, J. W. Storey, R. I. Thompson, D. P. van der Werf, J. S. Wurtele, and Y. Yamazaki (ALPHA Collaboration), Phys. Rev. Lett. **106**, 025002 (2011).

[42] N. Zurlo, M. Amoretti, C. Amsler, G. Bonomi, P. D. Bowe, C. Carraro, C. L. Cesar, M. Charlton, M. Doser, A. Fontana, M. C. Fujiwara, R. Funakoshi, P. Genova, J. S. Hangst, R. S. Hayano, L. V. Jorgensen, A. Kellerbauer, V. Lagomarsino, R. Landua, L. E. Rizzini, M. Macri, N. Madsen, G. Manuzio, D. Mitchard, P. Montagna, L. G. Posada, H. Pruys, C. Regenfus, A. Rotondi, G. Testera, D. P. Van der Werf, A. Variola, L. Venturelli, and Y. Yamazaki (ATHENA Collaboration), Phys. Rev. Lett. **97**, 153401 (2006).

[43] E. Lodi Rizzini *et al.* (ATHENA Collaboration), Eur. Phys. J. Plus **127**, 124 (2012).

[44] S. Maury, Hyperfine Interact. **109**, 43 (1997).

[45] T. Eriksson, Hyperfine Interact. **194**, 123 (2009).

[46] S. Maury *et al.*, Hyperfine Interact. **229**, 105 (2014).

[47] E. Lodi Rizzini, V. Mascagna, L. Venturelli, N. Zurlo, and M. Charlton, Hyperfine Interact. **228**, 53 (2014).

[48] L. Spitzer, *Physics of Fully Ionised Gases* (Interscience Publications, New York, 1956).

[49] J. L. Hurt, P. T. Carpenter, C. L. Taylor, and F. Robicheaux, J. Phys. B **41**, 165206 (2008).

[50] M. Amoretti *et al.*, Phys. Lett. A **360**, 141 (2006).